Radiation heat wave as a basic feature in laser-irradiated foils

R. F. Schmalz, J. Meyer-ter-Vehn, and R. Ramis*
Max-Planck-Institut für Quantenoptik, Postfach 1513, D-8046 Garching bei München, Federal Republic of Germany
(Received 28 February 1986)

Radiation hydrodynamics of laser-irradiated plane foils is studied numerically in the frequency-averaged diffusion approximation. Open and closed geometries are considered. It is shown that radiatively driven ablative heat waves play an important role for materials with medium atomic number Z and become dominant for high-Z matter. Scaling relations are given and the role of the opacity is pointed out.

I. INTRODUCTION

When a slab of matter is irradiated by a high-power laser pulse, the ablated material is heated to temperatures in the keV regime.[1] The deposited laser energy is transported into the cold material by a number of mechanisms such as electronic heat conduction, fast electrons, and radiation transport. Electronic heat conduction is extensively studied in the literature and seems to be fairly well understood despite the remaining problems connected with nonlocality and magnetic field effects.[2] Fast electrons can be avoided by choosing appropriate laser conditions, especially submicron wavelengths and moderate intensities. It is only recently, however, that radiation effects have been studied.[3–10] The importance of radiation transport processes was clearly pointed out in the work of Duston *et al.*,[9,10] who showed that already for lighter elements, such as aluminum and carbon, radiation effects have to be taken into account in order to describe the hydrodynamic motion of the material correctly.

For aluminum the following approximate picture emerges: the radiation consists of two parts, namely a hard component (mainly K-shell lines above 1 keV), which immediately penetrates thin foils, and a soft component (sub-keV), which is strongly absorbed and has to work its way through the foil diffusively. The hard component preheats the foil to a few eV via inner-shell ionization but may be ignored for most aspects of the hydrodynamics and energetics of the foil. The soft component, however, causes heating and ablation of a rather large portion of mass to moderate temperatures of around 50 eV. This is very important for the understanding of energy transport in medium and high-Z materials. The present paper is focused on this new feature, which was missing in former simulations of laser foil experiments.[11]

To obtain their results, Duston *et al.* used a very detailed line-transport procedure which appears to be prohibitively complicated for routine calculations such as are very often needed in the laboratory. It is therefore worthwhile to look for something simpler which can reproduce the main features of the underlying physics. A simple and comprehensive approach to this problem is the frequency-averaged (one-group or "grey") diffusion approximation assuming local thermodynamic equilibrium. In this paper, we report on results obtained within this model.

In Sec. II, we introduce the model and discuss the boundary conditions. In Sec. III some basic results on aluminum are presented. The dependence on the atomic number Z is investigated in Sec. IV. In Sec. V the scaling with laser intensity is shown, and a critical discussion of the model is given in Sec. VI. Section VII presents the summary and conclusions.

II. THE MODEL

We use an improved version of the MINIRA one-dimensional Lagrangian code.[12] It describes radiation diffusion coupled with hydrodynamic motion in a frequency-averaged approximation. It allows for two temperatures, namely a matter temperature T and a radiation temperature $T_{\rm rad}$ which is derived from the radiation energy density U according to

$$T_{\rm rad}=\left[\frac{U}{a}\right]^{1/4}$$

($a=137$ erg/cm^3/eV^4). The optical properties of the material are described by Rosseland and Planck mean opacities κ_R and κ_P, respectively (see the Appendix). Electronic heat conduction is included in Spitzer's form and laser energy deposition Q is modeled by inverse bremsstrahlung absorption and a 100% dump of the remaining energy at the critical density. The basic equations are

$$\frac{D\rho}{Dt}=-\rho\frac{\partial v}{\partial x}\ ,$$

$$\frac{Dv}{Dt}=-\frac{1}{\rho}\frac{\partial}{\partial x}(p+p_r)\ ,$$

$$\rho\frac{De}{Dt}=-p\frac{\partial v}{\partial x}-\frac{\partial q}{\partial x}-c\rho\kappa_P(U_P-U)+Q\ ,$$

$$\frac{D}{Dt}\left[\frac{U}{\rho}\right]=-\frac{p_r}{\rho}\frac{\partial v}{\partial x}-\frac{1}{\rho}\frac{\partial S}{\partial x}+c\kappa_P(U_P-U)\ ,$$

$$\frac{DS}{Dt}=-c^2\frac{\partial p_r}{\partial x}-c\rho\kappa_R S\ ,$$

where ρ and v are the density and velocity of the material, p its pressure, and e its specific internal energy. The radiation pressure is represented by p_r and the radiation ener-

gy density by U. Planck's equilibrium radiation energy density is given by

$$U_P = aT^4$$

($\sigma = 2\pi^5 k^4/15h^3c^2 = 1.03\times 10^{12}$ erg/s cm^2 eV^4 = Stefan-Boltzmann constant, k = Boltzmann's constant, h = Planck's constant, c = light velocity). The radiation flux is denoted by S and the electronic heat flux is given by

$$q = -\kappa_e T^{5/2}\frac{\partial T}{\partial x} .$$

In order to close the system of equations, the "Eddington factor" f is introduced by $p_r = fU$ ($\frac{1}{3} \le f \le 1$, we use $f = \frac{1}{3}$) and an equation of state $p = p(e,\rho)$ is specified. The latter is taken from the Los Alamos SESAME library.[13] When talking about radiation we always mean "soft x-ray radiation" and not the laser.

Two different boundary conditions for the radiation flux are applied. In the first one [Fig. 1(a)], referred to as "open geometry," radiation is allowed to leave both sides of the foil freely. Radiation losses are thus possible. This is a standard situation in laser foil experiments. Recently, however, there has been a growing interest in experiments where the laser shines on the inner surface of a hollow cavity, entering through a hole.[14,15] We approximate this case by two parallel walls with a slab cavity in between and assume that each wall element absorbs the same amount of laser light [Fig. 1(b)]. Owing to symmetry, the inner surface emits as much radiation as it receives from the opposite side so that the net radiation flux at the inner boundary is zero. We refer to this case as "closed geometry." In the following, we show results for both open and closed geometry.

III. BASIC RESULTS

In order to discuss the typical outcome of a code run, we consider the following case: An aluminum foil 1.5-μm thick is irradiated with 1.3-μm wavelength laser light of 10^{13} W/cm^2 intensity and 0.3 ns (FWHM) pulse length (open geometry). This is typical of the ASTERIX III iodine laser at Max-Planck-Insitut für Quantenoptik in Garching. Equation of state data as well as Rosseland and Planck mean opacities required as input by the code are taken in tabular form from the SESAME equation-of-state and opacity library.[13] An example of the structure of these data is given in the appendix.

The code results are conveniently represented in the form of three-dimensional (3D) diagrams where the physically interesting quantities are plotted versus mass coordinate and time. In Figs. 2 and 3 we show the matter temperature T and the density in logarithmic representation up to the time 1.5 ns. The laser light comes from the right. Three different regions are clearly visible in Fig. 2. First, there is the relatively small, hot outer region with

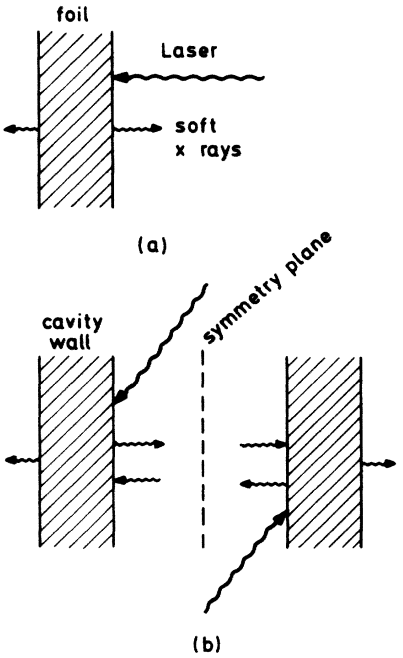

FIG. 1. Illustration of the boundary conditions. (a) Open geometry: soft-x-ray radiation can freely leave the foil boundaries. (b) Closed geometry: laser light uniformly illuminates the inner surface of two parallel foils which form the walls of a slab cavity. Only one slab is simulated and the presence of the cavity is replaced by the boundary condition of vanishing radiation flux at its right boundary. By symmetry, this corresponds to the situation shown.

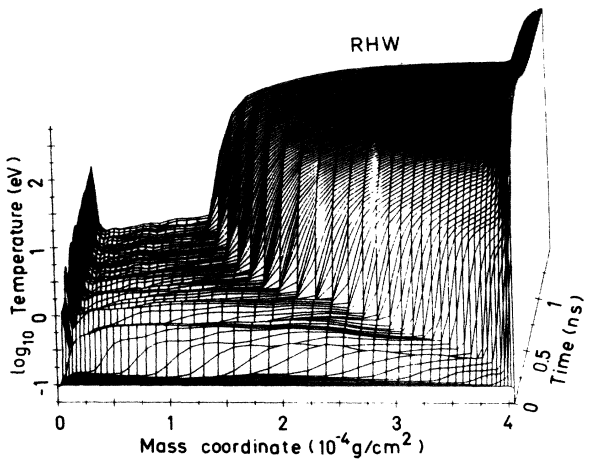

FIG. 2. Matter temperature vs the mass coordinate and time for a typical code run. The laser light comes from the right, its parameters are: intensity 10^{13} W/cm^2, pulse duration 0.3 ns, wavelength 1.3 μm. The target is 1.5 μm aluminum. The actual computational mesh is shown on the mass coordinate, indicating the fine zoning at the boundaries. From right to left, three different plateaulike regions are seen: the hot corona, the radiation heat wave, and the cold shock-heated matter. The spike at the left boundary is generated by the shock waves running into the expanding material.

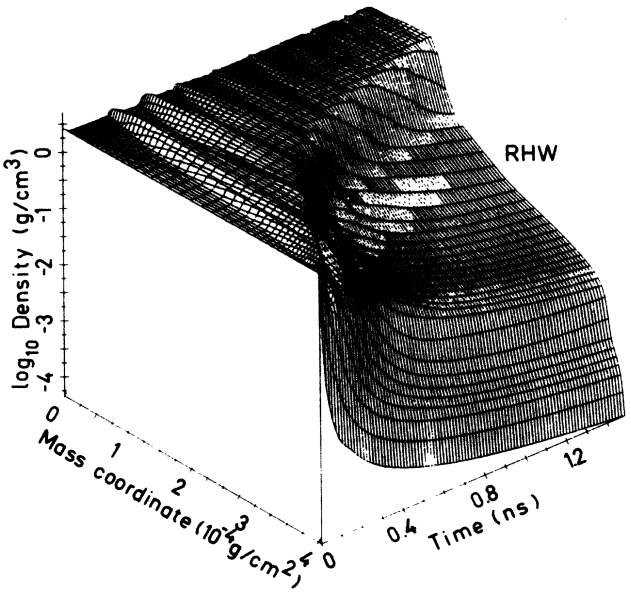

FIG. 3. Density vs mass coordinate and time for the case of Fig. 2. The region of the ablative radiation heat wave (RHW) is marked.

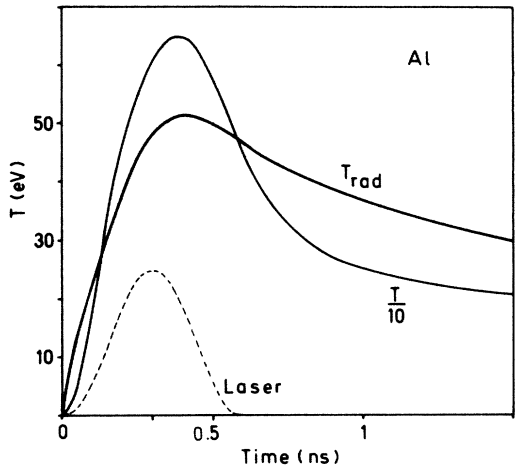

FIG. 4. Maximum matter temperature T (reduced by a factor of 10) and radiation temperature T_{rad} in aluminum versus time for the conditions of Fig. 2. The laser pulse is added in arbitrary units (sine square shape).

temperatures of around 600 eV. This includes the critical density and will be called corona in the following. Second, a large, moderately heated region around 50 eV, and third, the cold shock-heated material at roughly 1 eV. The same three regions are seen in the density plot in Fig. 3. The second region represents the basic new feature of these calculations. It is a nonlinear *radiation heat wave* (RHW) generated by the diffusion of radiation into the cold material. The basic mechanism of this wave can be understood in terms of (nonlinear) radiation heat conductivity as described in the book of Zel'dovich and Raizer.[16] Simplified descriptions in form of self-similar solutions have been given by, for example, Marshak[17] and, more recently, by Pakula and Sigel.[18,19] The RHW causes the ablation of a considerable amount of mass, as can be seen from Fig. 3, and has dramatic consequences on the characteristics of laser-irradiated foils.

The temporal behavior of the matter and radiation temperatures are plotted in Fig. 4. The spatial maxima of both quantities are shown. The laser pulse is added for comparison. It is seen that the maxima of the matter temperature T and radiation temperature T_{rad} come slightly later than the pulse maximum. The decay time of the radiation temperature is considerably longer than that of the matter temperature. Energy is thus stored for a longer time in the RHW.

The question now arises to what extent can one trust this simple one-group description. To answer this question, we made a detailed comparison with Ref. 9, where a much more elaborate line-transport procedure is applied. It shows that our model affords a quite good reproduction of the profiles of density and temperature given there. This is seen from Fig. 5, where we have plotted MINIRA results (solid lines, 10^{13} W/cm^2, 3-ns pulse, $\lambda=1$ μm, 8-μm Al foil) on top of the profiles of Ref. 9 (dashed) in Eulerian coordinates at peak radiation temperature. The matter temperature, density, and radiation emission ($\partial S/\rho\partial x$) are shown as well as the location of the critical density x_c. Since the scale for the radiation emission given in Ref. 9 seems to be in error, we have fitted these values to our results at the point of peak emission. We notice that our code gives a somewhat more pronounced structure than that of Ref. 9 which is clearly a conse-

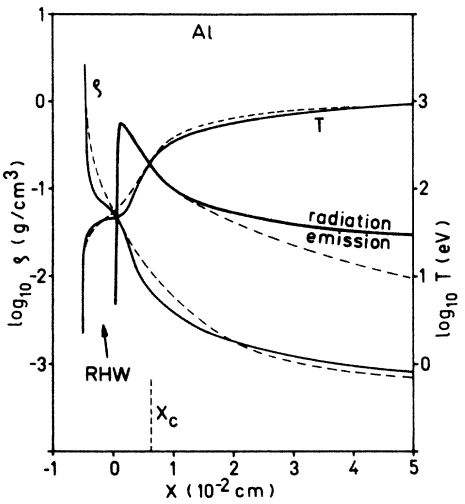

FIG. 5. Comparison of MINIRA results (solid lines) with Duston *et al.* (Ref. 9, dashed lines). Compared are the profiles of matter temperature T, density ρ, and radiation emission (units W/g) at the time of maximum radiation temperature ($\approx$4 ns). Laser parameters: wavelength = 1 μm, pulse duration = 3 ns, intensity = 10^{13} W/cm^2; target: 8 μm aluminum. Apparently, the scale for the radiation emission in Ref. 9 is in error, therefore this curve is fitted to the maximum of our curve.

quence of the grey approximation: Different frequency groups having different mean-free paths tend to smear out the profiles. However, the overall coincidence is nearly quantitative. The sharp rise of the radiation emission curve clearly marks the base of the RHW.

The energy partition in the foil is also reproduced quite well. We find at the end of the run (8 ns): kinetic energy 45% (Ref. 9: 40.8%); internal energy 28% (Ref. 9: 32.8%); radiative loss 27% (Ref. 9: 26.4%).

A second comparison was made for carbon ($Z=6$) with Ref. 10. The results were quite similar to the aluminum case. We conclude that the basic physical processes can be understood in terms of a radiatively driven ablative heat wave in addition to the well-known corona and shock-wave physics.

IV. MATERIAL DEPENDENCE

The RHW is strongly material dependent. The determining quantity is the atomic number Z. For very light elements such as hydrogen the RHW is not visible. It starts to be recognized around $Z=6$ (carbon) and becomes dominant for high Z. Figure 6 shows the dependence of various quantities on Z, with T being the maximum material temperature, $T_{\rm rad}$ the maximum radiation temperature, p the maximum ablation pressure, and m the total ablated mass including the RHW. The laser intensity and pulse duration are fixed at our standard conditions (10^{13} W/cm^2, 0.3-ns pulse). The Z dependence is exemplified in closed geometry; in open geometry it looks qualitatively similar. The difference can be estimated from Sec. V.

Clearly visible on this plot is the onset of radiation effects, which start to dominate the pressure and temperature near $Z=13$ (aluminum). The presence of the RHW increases the ablation pressure by a factor of approximately 3 and dramatically cools the corona. Without radiation, the temperature would even slightly increase with Z and the ablation pressure would stay roughly constant.[11]

The actual runs were made for the materials given at the top. The last entry is for gold, $Z=79$. Because there are no opacity tables for gold in the SESAME library, we use two limits and give error bars. The lower limit is given by the opacity of the highest-Z element contained in the SESAME library, namely europium ($Z=63$). The higher limit is given by the maximum opacity theorem[20]

$$\kappa_{\rm lim}=\frac{Z}{A}\left[\frac{13.6\ {\rm eV}}{kT}\right]\times 4.57\times 10^5\ {\rm cm}^2/{\rm g}$$

(A=atomic weight). The large error bars indicate the uncertainties for high-Z elements such as gold because of the missing opacity information. Nevertheless, we use gold in the following instead of europium as an example of a high-Z material because of its higher practical importance. A simple opacity estimate is adopted [$\kappa_R=\kappa_P=(\kappa_{\rm lim}/6)$, see the Appendix] which corresponds to a continuous extrapolation of the curves in Fig. 6. However, we keep in mind that this may be unrealistic.

The main differences between a medium-Z element such as aluminum and a high-Z element such as gold become clear from Figs. 7 and 8. Here we plot the profiles of matter temperature, density, pressure, radiation temperature, and optical depth

$$\tau(x)=\int_0^x \frac{1}{l_R}dx\ ,$$

where $l_R=(1/\rho\kappa_R)$ versus the mass coordinate in open geometry under standard conditions. It is seen that the importance of the corona decreases as Z increases. The

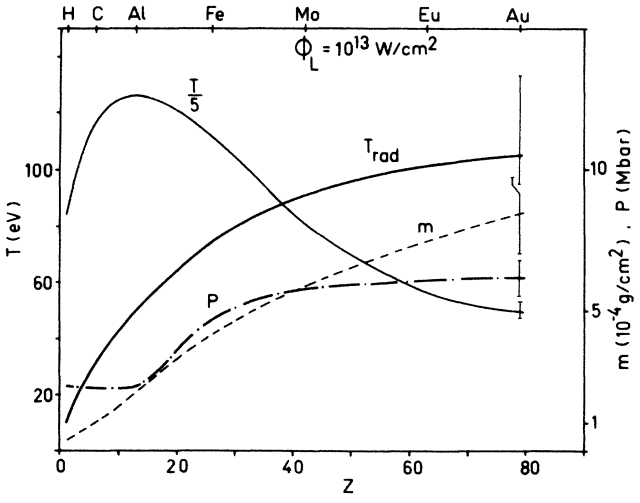

FIG. 6. Dependence of maximum matter temperature T (reduced by a factor of 5), maximum radiation temperature $T_{\rm rad}$, maximum ablation pressure p, and ablated mass m on the atomic charge number Z.

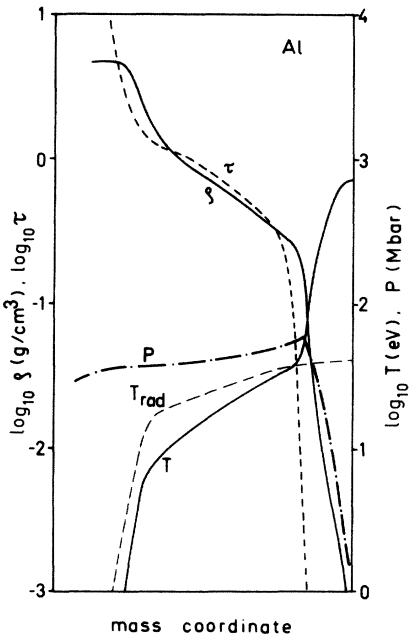

FIG. 7. Profiles of matter temperature ($\log T$), radiation temperature ($\log T_{\rm rad}$), density ($\log\rho$), optical depth ($\log\tau$, counted from the right), and pressure p vs mass coordinate for aluminum under the conditions of Fig. 2 (open geometry, time 0.4 ns).

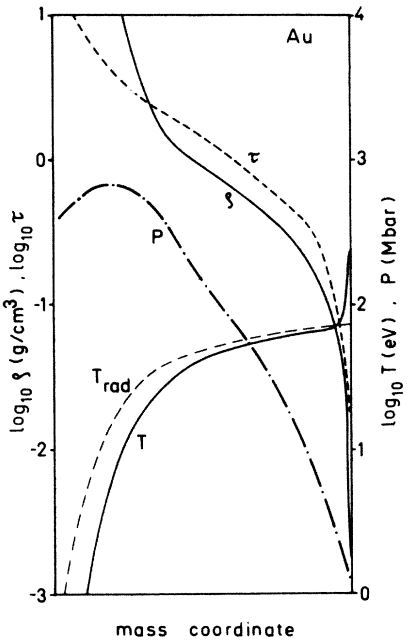

FIG. 8. Same as for Fig. 7, but for gold.

RHW dominates for high Z and attains temperatures of around 100 eV. The pressure in the interior of the RHW is roughly constant for aluminum but considerably increases for gold. The acceleration of the matter is thus strongly enhanced for gold[21] but not for aluminum. The corona is optically thin and the radiation temperature stays constant there. In the RHW region the radiation temperature always slightly exceeds the matter temperature. This is natural because the radiation drives the heat wave. The optical depth increases from roughly 0.1 at the base to 10 at the front of the RHW.

An important point is the partition of the laser energy into the various channels of kinetic, thermal, and radiation energy in corona and RHW. First of all, we notice that the energy stored in the radiation field is always negligible. For aluminum, the corona is not very different from that without a RHW for our standard conditions. In this case the RHW plays a minor role in the energy balance and almost all the energy resides in the corona. For gold, however, in closed geometry roughly 70% of the energy go into the RHW, mainly in the form of thermal energy. The corona contains 30%, equally distributed to the kinetic and thermal energies (at pulse maximum).

In open geometry we find 10% radiation losses for aluminum and 70% for gold. These numbers may be compared with x-ray conversion efficiencies as measured in experiments.[22–24] The agreement is quantitative for aluminum but not for gold, where the experimental value is around 40%. Possible reasons for this discrepancy are discussed in Sec. VI.

V. SCALING RELATIONS

Dimensional considerations lead to scaling laws. These are given in Ref. 18 in connection with the derivation of a self-similar solution for the radiatively driven ablative heat wave (in the radiation conduction approximation $T=T_{\rm rad}$). For example, if the flux S_0 at the boundary is given and the opacity is assumed to be proportional to $\kappa_{\rm lim}$, the scaling is

$$T\sim S_0^{4/13},\quad p\sim S_0^{10/13},\quad m\sim S_0^{7/13},$$

(in the notation of Ref. 18, the parameters are $\lambda=\frac{7}{3}$, $\mu=1$, $\delta=\frac{3}{2}$). Although we do not use the radiation conduction approximation, these scaling laws should be approximately valid in our gold case, too. This is because the coupling between the laser and radiation flux

$$S_0=\eta\Phi_L$$

is efficient ($\eta\approx 1$) and the corona plays a minor role. Figure 9 shows the results of MINIRA calculations for gold in closed geometry at peak radiation temperature ($\kappa_R=\kappa_P=\kappa_{\rm lim}/6$). In fact, the above scaling is realized in a wide range of laser intensities. The simulation results for gold in closed geometry are

$$T_{\rm rad}=100\left[\frac{\Phi_L}{10^{13}\ \mathrm{W/cm^2}}\right]^{0.3}\ \mathrm{eV},$$

$$p=8\left[\frac{\Phi_L}{10^{13}\ \mathrm{W/cm^2}}\right]^{0.78}\ \mathrm{Mbar},$$

$$m=1.2\times 10^{-3}\left[\frac{\Phi_L}{10^{13}\ \mathrm{W/cm^2}}\right]^{0.5}\ \mathrm{g/cm^2}.$$

These scalings are not so far from the ones given in Ref. 5, although the derivation is different there.

In open geometry, we obtain for gold

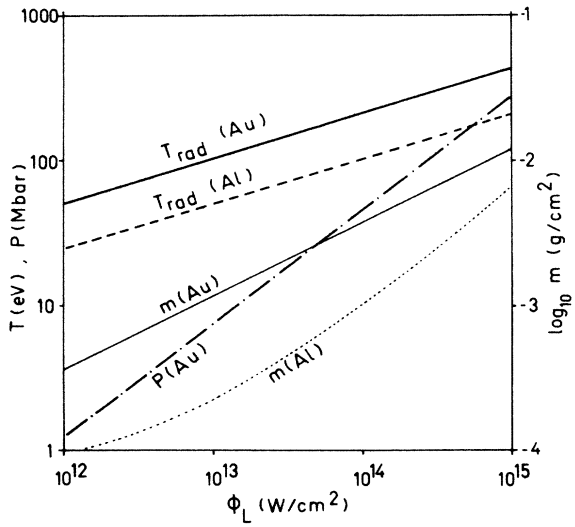

FIG. 9. Maximum radiation temperature $T_{\rm rad}$, ablation pressure p, and total ablated mass m vs laser intensity Φ_L for closed geometry. Solid lines represent gold, dashed lines aluminum.

$$T_{\rm rad}=73\left[\frac{\Phi_L}{10^{13}\ {\rm W/cm^2}}\right]^{0.27}\ {\rm eV}\ ,$$

$$p=3.2\left[\frac{\Phi_L}{10^{13}\ {\rm W/cm^2}}\right]^{0.7}\ {\rm Mbar}\ ,$$

$$m=6\times10^{-4}\left[\frac{\Phi_L}{10^{13}\ {\rm W/cm^2}}\right]^{0.47}\ {\rm g/cm^2}\ .$$

The reason for this weaker coupling is clearly the increase of radiation losses which behave roughly as $\sim\Phi_L^{0.23}$ $\sim(1-\eta)$.

For comparison, the behavior of aluminum is also shown in Fig. 9. The radiation temperature obviously obeys the same intensity scaling as for gold but with absolute values just half as big. However, the same is not true of the maximum pressure and the ablated mass, which do not obey a simple power law. This is illustrated by the dotted line in Fig. 9, which represents the total ablated mass for aluminum. Besides the fact that aluminum is still dominated by the corona having a different scaling, another effect seems to arise, namely the shock heating becomes non-negligible at higher laser intensities. Shock temperatures of around 100 eV are generated which dramatically reduces the opacity of the foil before the RHW develops. Ultimately, this leads to another interesting regime (beyond 10^{15} W/cm^2) where the RHW catches up with the shock wave. This goes beyond the scope of the present paper and will be discussed elsewhere.

Finally, we mention the dependence of our results on the laser wavelength. Shorter wavelengths generally tend to thicken the corona and to reduce its temperature. This could influence the coupling to the RHW. For aluminum, the code predicts a noticeable increase of the radiation temperature and the conversion efficiency for submicron wavelengths. For gold, however, we find nearly no dependence of these quantities on wavelength. This may be due to the poor description of the gold corona in open geometry, as discussed in the next section.

VI. DISCUSSION

One of the goals of this paper was to investigate the capability of the rather simple frequency-averaged radiation diffusion model for the description of laser foil ablation. The advantages of this approach are obvious: it is fast, compact, and conceptually simple. Furthermore, it appears that there is remarkable agreement with much more sophisticated radiation transport models for medium-Z materials such as aluminum concerning the coupling of radiation with hydrodynamics and, in particular, the formation of a well-defined radiation heat wave. On the other hand, the model has obvious shortcomings and may lead to incorrect results in certain aspects. These are now discussed in order to identify those questions for which the simplified model can give reliable answers.

One weak point in the model presented here is the description of the corona. The assumption of local thermodynamic equilibrium (LTE) is appropriate for the dense, collision-dominated plasma in the RHW region, but tends to overestimate the radiation emission and therefore the radiative cooling of the corona region, in particular for high-Z materials. It has been pointed out (for example, in Ref. 25) that a non-LTE description may be essential for the corona. As a result, our model possibly predicts too high conversion efficiences and too low corona temperatures for gold. Nevertheless, the results for aluminum compare surprisingly well with experiments.

Since the focus of this paper is on questions of radiation hydrodynamics such as ablation rate and pressure, acceleration of foils, etc., but not on details of the corona physics, the main deficiency of the model lies in the overestimating radiation losses and, as a consequence, insufficient coupling of the laser energy into the dense parts of the foil. This criticism is correct for open geometry. However, it does not hold to the same extent for the closed geometry as long as there is no net energy loss into the cavity. We therefore expect that the results presented here for high-Z materials are more reliable for closed geometry.

Another shortcoming of our simulation concerns preheat effects due to fast electrons and hard x-ray radiation. Hot electrons appear only at high laser intensities and long wavelengths. We therefore do not need to take it into account under the standard conditions considered here. Radiation preheat can be estimated from Ref. 9. There a maximum rear-side temperature of the 8 μm aluminum foil of nearly 8 eV is found. Energetically, this effect is quite small and does not lead to severe dynamic consequences. Furthermore, the hard component of the radiation strongly varies with the material and may be considerably weaker than for aluminum.[23] We therefore do not expect noticeable effects on our conclusions.

Furthermore, as was already mentioned, the opacities we used for high-Z elements such as gold may be unrealistic. The strong opacity dependence of our results on the other hand suggests that the feasibility of opacity measurements with lasers be investigated.

Finally, as an application, a two-step procedure is proposed (and used in Ref. 26) in order to obtain radiative spectra: First, the profiles are generated in the grey approximation and line transport is added by post-processing.

VII. SUMMARY AND CONCLUSIONS

High-power laser ablation of plane foils was studied numerically by means of the MINIRA one-dimensional Lagrangian code. Radiation transport was included in a frequency-averaged (grey) diffusion approximation. Open and closed geometries were considered by choosing appropriate boundary conditions.

First, by comparison with other work, it is shown that most of the characteristic new features that appear in the density and temperature profiles of aluminum may be attributed to the existence of a radiation-driven (Marshak type) ablative heat wave.

These waves are important for medium-Z materials and turn out to be dominant for high Z. Uncertainties remain for very high-Z elements such as gold. The reasons for this are discussed and the importance of the opacity is

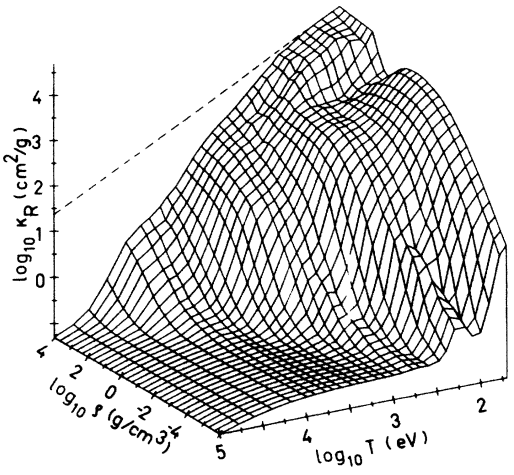

FIG. 10. SESAME Rosseland opacities vs temperature and density for europium ($Z=63$). The dashed line is given by the maximum opacity theorem.

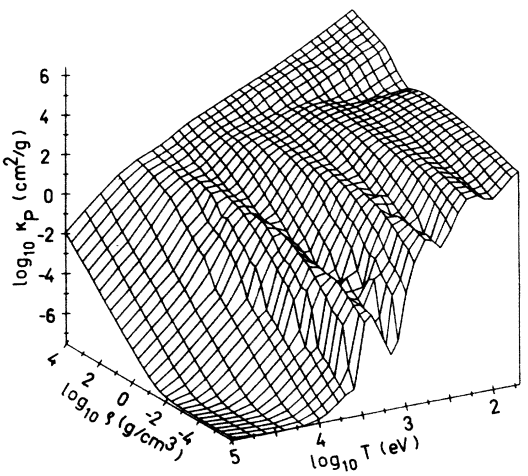

FIG. 11. SESAME Planck opacities vs temperature and density for europium.

pointed out.

Scaling relations are given and compared with simple analytical models. Good agreement is found in cases where they are applicable, i.e., where the corona plays a minor role. The limitations of the model are discussed.

In conclusion, the paper helps to clarify the physical nature of important new features in the problem of high-power laser light coupling to matter and opens a method of finding quick answers to those questions of radiation hydrodynamics where spectral resolution is not needed.

ACKNOWLEDGMENTS

This work was supported in part by the Commision of the European Communities in the framework of the Association EURATOM—Max-Planck-Institut für Plasmaphysik and by the Bundesministerium für Forschung und Technologie (Bonn, Germany).

APPENDIX

The definition of the Rosseland opacity is

$$\frac{1}{\kappa_R}=\frac{\int_0^\infty \frac{1}{\kappa_\nu}\frac{\partial U_{\nu p}}{\partial T}d\nu}{\int_0^\infty \frac{\partial U_{\nu p}}{\partial T}d\nu}$$

with the Planck function

$$U_{\nu p}=\frac{8\pi h\nu^3}{c^3}\frac{1}{e^{h\nu/kT}-1}\ .$$

$U_{\nu p}$ has its maximum at $h\nu=2.8$ kT, while the weighting function $\partial U_{\nu p}/\partial T$ peaks at $h\nu\approx 4$ kT.

The Planck opacity is defined as

$$\kappa_P=\frac{\int_0^\infty \kappa_\nu U_{\nu p}\,d\nu}{\int_0^\infty U_{\nu p}\,d\nu}\ .$$

The SESAME opacity library provides tables of Rosseland and Planck opacities for most materials up to $Z=63$ (europium). The way in which these tables are generated is unknown to us. Figures 10 and 11 show 3D plots of the europium Rosseland and Planck opacities, respectively. In Fig. 10, the maximum opacity $\kappa_{\rm lim}$ (defined in Sec. IV) is indicated by the dashed line. Obviously, this is built in the tables as a limit for high densities and low temperatures.

We expect the gold opacity to be higher than that for europium. Therefore, by comparison with europium in the interesting temperature region of around 100 eV and densities of around 1 g/cm^3, a reasonable approximation for gold could be

$$\kappa_R\approx\frac{\kappa_{\rm lim}}{6}\ .$$

This is not more than an educated guess and reflects our present knowledge.

*Permanent address: Escuela Técnica Superior de Ingenieros Aeronaúticos, Universidad Politécnica de Madrid, E-28006 Madrid, Spain.

[1]K. Eidmann, F. Amiranoff, R. Fedosejevs, A. G. M. Maaswinkel, R. Petsch, R. Sigel, G. Spindler, Yung-lu Teng, G. Tsakiris, and S. Witkowski, Phys. Rev. A 30, 2568 (1984).

[2]J. F. Luciani, P. Mora, and A. Bendib, Phys. Rev. Lett. 55, 2421 (1985).

[3]T. J. Goldsack, J. D. Kilkenny, B. J. McGowan, P. F. Cunningham, C. S. Lewis, M. H. Key, and P. T. Rumsby, Phys. Fluids 25, 1634 (1982).

[4]W. C. Mead, E. M. Campbell, K. G. Estabrook, R. E. Turner,

W. L. Kruer, P. H. Y. Lee, B. Pruett, V. C. Rupert, K. G. Tirsell, G. L. Stradling, F. Ze, C. E. Max, M. D. Rosen, and B. F. Lasinski, Phys. Fluids **26**, 2316 (1983).

[5]T. Yabe, S. Kiyokawa, T. Mochizuki, S. Sakabe, and C. Yamanaka, Jpn. J. Appl. Phys. **22**, L88 (1983).

[6]B. Yaakobi, J. Delettrez, L. M. Goldman, R. L.McCrory, R. Marjoribanks, M. C. Richardson, D. Shvarts, S. Skupsky, J. M. Soures, C. Verdon, D. M. Villeneuve, T. Boehly, R. Hutchinson, and S. Letzring, Phys. Fluids **27**, 516 (1984).

[7]A. Ng, D. Parfeniuk, L. DaSilva, and D. Pasini, Phys. Fluids **28**, 2915 (1985).

[8]H. Pepin, R. Fabbro, B. Faral, F. Amiranoff, J. Virmont, F. Cottet, and J. P. Romain, Phys. Fluids **28**, 3393 (1985).

[9]D. Duston, R. W. Clark, J. Davis, and J. P. Apruzese, Phys. Rev. A **27**, 1441 (1983).

[10]D. Duston, R. W. Clark, and J. Davis, Phys. Rev. A **31**, 3220 (1985).

[11]R. F. Schmalz and J. Meyer-ter-Vehn, Phys. Fluids **28**, 932 (1985).

[12]K. Unterseer and J. Meyer-ter-Vehn, Max-Planck-Institut für Quantenoptik Report No. MPQ **82**, 1985 (unpublished).

[13]T4-Group, Los Alamos National Laboratory Report No. LALP-83-4, 1983 (unpublished).

[14]K. Okada, T. Mochizuki, N. Ikeda, M. Hamada, M. Mineo, R. Kodama, and C. Yamanaka, J. Appl. Phys. **59**, 2332 (1986).

[15]R. Pakula and R. Sigel, Max-Planck-Institut für Quantenoptik Report No. MPQ 85, 1985 (unpublished).

[16]Ya. B. Zel'dovich and Yu. P. Raizer, *Physics of Shock Waves and High-Temperature Hydrodynamic Phenomena* (Academic, New York, 1966).

[17]R. E. Marshak, Phys. Fluids **1**, 24 (1957).

[18]R. Pakula and R. Sigel, Phys. Fluids **28**, 232 (1985).

[19]J. Meyer-ter-Vehn, R. Pakula, R. Sigel, and K. Unterseer, Phys. Lett. **104A**, 410 (1984).

[20]J. Bernstein and F. J. Dyson, General Atomics Report No. GA-848, 1959 (unpublished).

[21]I. B. Földes, K. Koyama, R. Sigel, G. D. Tsakiris, A. Böswald, Chen Shi-sheng, A. G. M. Maaswinkel, R. F. Schmalz, and S. Witkowski, Europhys. Lett. (to be published).

[22]W. C. Mead, E. M. Campbell, K. G. Estabrook, R. E. Turner, W. L. Kruer, P. H. Y. Lee, B. Pruett, V. C. Rupert, K. G. Tirsell, G. L. Stradling, F. Ze, C. E. Max, and M. D. Rosen, Phys. Rev. Lett. **47**, 1289 (1981).

[23]T. Mochizuki, T. Yabe, K. Okada, M. Hamada, N. Ikeda, S. Kiyokawa, and C. Yamanaka, Phys. Rev. A **33**, 525 (1986).

[24]T. Kishimoto, Max-Planck-Institut für Quantenoptik Report No. MPQ 108, 1985 (unpublished).

[25]S. Kiyokawa, T. Yabe, and T. Mochizuki, Jpn. J. Appl. Phys. **22**, L772 (1983).

[26]G. D. Tsakiris, P. Herrmann, R. Pakula, R. Schmalz, R. Sigel, and S. Witkowski, Europhys. Lett. (to be published).

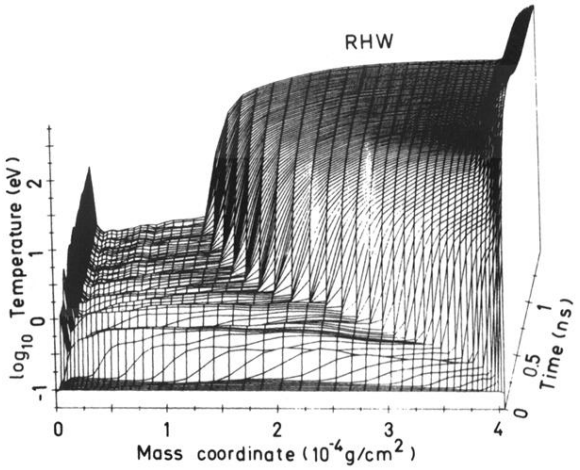

FIG. 2. Matter temperature vs the mass coordinate and time for a typical code run. The laser light comes from the right, its parameters are: intensity 10^{13} W/cm^2, pulse duration 0.3 ns, wavelength 1.3 μm. The target is 1.5 μm aluminum. The actual computational mesh is shown on the mass coordinate, indicating the fine zoning at the boundaries. From right to left, three different plateaulike regions are seen: the hot corona, the radiation heat wave, and the cold shock-heated matter. The spike at the left boundary is generated by the shock waves running into the expanding material.

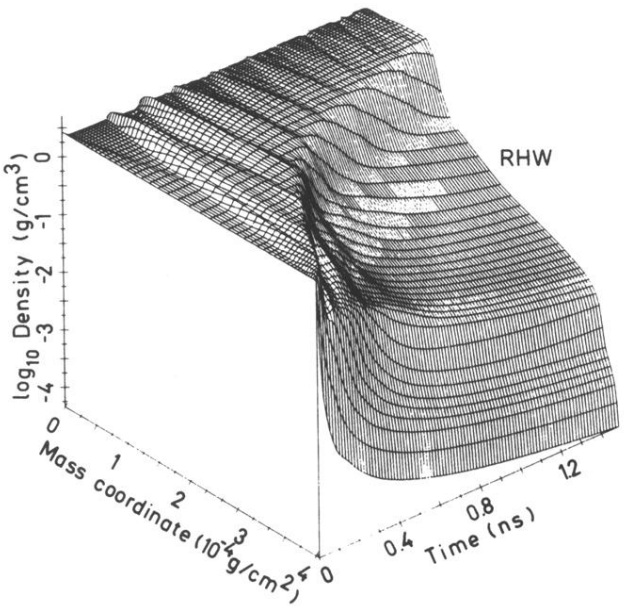

FIG. 3. Density vs mass coordinate and time for the case of Fig. 2. The region of the ablative radiation heat wave (RHW) is marked.